Mon. Not. R. Astron. Soc. **384,** 1733–1740 (2008) doi:10.1111/j.1365-2966.2008.12863.x

A populous intermediate-age open cluster and evidence of an embedded cluster among the FSR globular cluster candidates

E. Bica★ and C. Bonatto

Departamento de Astronomia, Universidade Federal do Rio Grande do Sul Av. Bento Gonçalves 9500, Porto Alegre 91501-970 RS, Brazil

Accepted 2007 December 17. Received 2007 December 13; in original form 2007 November 15

ABSTRACT

We study the nature of the globular cluster (GC) candidates FSR 1603 and FSR 1755 selected from the catalogue of Froebrich, Scholz & Raftery. Their properties are investigated with Two-Micron All-Sky Survey field-star decontaminated photometry, which is used to build colour–magnitude diagrams (CMDs) and stellar radial density profiles. FSR 1603 has the open cluster Ruprecht 101 as optical counterpart, and we show it to be a massive intermediate-age cluster. Relevant parameters of FSR 1603 are the age ≈1 Gyr, distance from the Sun $d_{\odot} \approx 2.7$ kpc, Galactocentric distance $R_{\rm GC} \approx 6.4$ kpc, core radius $R_{\rm C} \approx 1.1$ pc, mass function slope $\chi \approx 1.8$, observed stellar mass (for stars with mass in the range $1.27 \leqslant m \leqslant 2.03\,{\rm M}_{\odot}$) $M_{\rm obs} \approx 500\,{\rm M}_{\odot}$ and a total (extrapolated to $m = 0.08\,{\rm M}_{\odot}$) stellar mass $M_{\rm tot} \approx 2300\,{\rm M}_{\odot}$. FSR 1755, on the other hand, is not a populous cluster. It may be a sparse young cluster embedded in the H II region Sh 2-3, subject to an absorption $A_V \approx 4.1$, located at $d_{\odot} \approx 1.3$ kpc. Important field-star contamination, spatially variable heavy dust obscuration, even in $K_{\rm s}$, and gas emission characterize its field. A nearly vertical, sparse blue stellar sequence shows up in the CMDs.

Key words: open clusters and associations: general – Galaxy: structure.

1 INTRODUCTION

A catalogue containing 1021 star cluster candidates for Galactic latitudes $|b| < 20^{\circ}$ and all longitudes was recently published by (Froebrich et al. 2007b, hereafter FSR). Their targets (FSR objects) were detected by means of an automated algorithm that basically identified regions with stellar overdensities, applied to the Two-Micron All-Sky Survey (2MASS)[1] data base. The overdensities were classified according to a quality flag, '0' and '1' representing the most probable star clusters, while the '5' and '6' flags may be related to field fluctuations.

By means of a combination of three parameters, the number of cluster stars corrected to a common magnitude limit, the core radius and the central star density, FSR could discriminate known globular clusters (GCs) from open clusters (OCs). When applied to the catalogue, this criterion led them to classify 1012 targets as OC candidates and nine as GC candidates that should be explored in follow-up studies. Among the latter are FSR 1603 and FSR 1755.

Several works have already explored the FSR catalogue with varying depths and different approaches, with results that reflect the importance of such catalogue. The recently discovered GCs FSR 1735 (Froebrich, Meusinger & Scholz 2007a) and FSR 1767 (Bonatto et al. 2007), and the probable GCs FSR 584 (Bica et al. 2007a) and FSR 190 (Froebrich, Meusinger & Davis 2008), are clear examples of the fundamental role played by the FSR catalogue to improve the statistics of very old star clusters. Indeed, FSR 1735 and FSR 1767 are the most recent additions to the Galactic GC population, a number that presently amount to ∼160 members (e.g. Bonatto & Bica 2007c).

Besides the obvious importance of finding new star clusters of any age throughout the Milky Way, the identification of the intermediate-age clusters (IACs) FSR 31, FSR 89 and FSR 1744, projected towards the centre of the Galaxy (Bonatto & Bica 2007a), has provided as well important information on cluster disruption processes and survival rates in those regions. In this context, derivation of astrophysical parameters of new star clusters can be used in studies related to the star formation and evolution processes, dynamics of *N*-body systems, cluster disruption time-scales, the geometry of the Galaxy, among others.

Central to the problem of identifying the nature of catalogue stellar overdensities is the availability of a field-star decontamination algorithm to disentangle physical colour–magnitude diagrams (CMD) sequences from field fluctuations. Low-noise stellar radial density profiles (RDPs) spanning a wide-radial range are essential as well, especially for objects projected against dense stellar fields (e.g. Bonatto & Bica 2007b). For instance, based on such premises and working with the decontamination algorithm described in Bonatto & Bica (2007b) applied to 2MASS photometry, Bonatto & Bica (2007a) found that the GC candidate FSR 89 is rather a well-defined IAC.

Most of the FSR catalogue remains to be further explored. As another step in the direction of classifying FSR candidates – taking

★E-mail: bica@if.ufrgs.br (EB); charles@if.ufrgs.br (CB)

[1] The 2MASS, available at www.ipac.caltech.edu/2mass/releases/allsky/.

Table 1. Data from FSR

Object	α (2000) (^{h} ^{m} ^{s})	δ (2000) ($^\circ$ $'$ $''$)	ℓ ($^\circ$)	b ($^\circ$)	R_C (arcmin)	R_t (arcmin)	Classification	Quality flag	$N_c(H=15)$ (stars)
(1)	(2)	(3)	(4)	(5)	(6)	(7)	(8)	(9)	(10)
FSR 1603	12:09:45	−62:59:49	298.22	−0.51	1.1	29.6	Probable	0	1842
FSR 1755	17:12:20	−38:27:44	348.25	+0.48	3.2	6.4	Probable	2	90

Notes. Columns 2 and 3: central coordinates. Columns 4 and 5: corresponding Galactic coordinates. Columns 6 and 7: Core and tidal radii derived from King fits to the 2MASS H images. Column 8: both candidates have been considered as probable star clusters. Column 9: FSR quality flag. Column 10: number of prospective cluster members, corrected to $H = 15$.

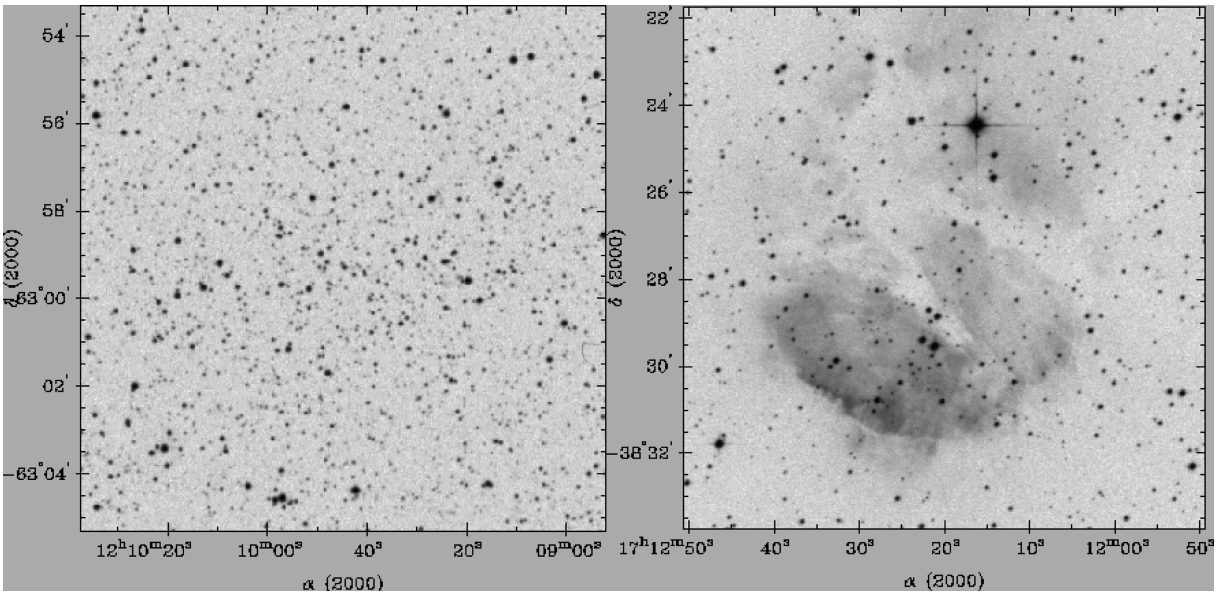

Figure 1. Left-hand panel: 12 × 12 arcmin^2 DSS B image of FSR 1603. Right-hand panel: 12 × 12 arcmin^2 XDSS R image of FSR 1755, where gas emission and strong dust absorption are conspicuous. Images centred on the FSR coordinates (columns 2 and 3 of Table 1).

into account CMD and RDP properties – we show in this work that the candidates, FSR 1603 and FSR 1755, are not GCs. Instead, FSR 1603 is a massive IAC projected ∼60° from the centre of the Galaxy, and FSR 1755 is an embedded cluster ∼12° from the centre.

This paper is structured as follows. In Section 2, we present fundamental data and optical and near-infrared (near-IR) images of FSR 1603 and FSR 1755. In Section 3, we present the 2MASS photometry and discuss the methods employed in the CMD analyses, especially the field-star decontamination and the stellar radial density profiles. In Section 4, we apply the tools to both candidates and discuss their nature. Concluding remarks are given in Section 5.

2 THE GC CANDIDATES FSR 1603 AND FSR 1755

Table 1 provides original information on FSR 1603 and FSR 1755, where we also include the core and tidal radii measured by FSR in the 2MASS H images by means of a King (1962) profile fit. Both candidates have been classified as probable star clusters by FSR; the quality flags are also given. The different quality flags of FSR 1603 and FSR 1755 can be accounted for by the significantly different numbers of prospective cluster members computed by FSR, which we include in the last column of Table 1.

FSR 1603 has the OC Ruprecht 101 as optical counterpart, for which the coordinates are the only data provided by the WEBDA[2] data base. The relatively low contrast of FSR 1603 with respect to the background can be seen in the 12 × 12 arcmin^2 Digital Sky Survey (DSS).[3] Nevertheless, a few bright stars appear to stand out around the image centre over a rather uniform stellar background.

The field of FSR 1755, on the other hand, presents a complex structure that includes important contamination by bulge stars, strong absorption by dust lanes and Hα emission, clearly seen in the 12 × 12 arcmin^2 Second Generation Digital Sky Survey (XDSS) R image (Fig. 1, left-hand panel). These features show up as well in the near IR, as can be seen in the 2MASS K_s images (Fig. 2), in two different spatial scales. Note the presence of a bright O star about 2 arcmin to the south of the central coordinates of FSR 1755 (Section 4.2).

3 PHOTOMETRY AND ANALYTICAL TOOLS

In this section, we briefly describe the photometry and outline the methods we apply in the CMD analyses.

[2] obswww.unige.ch/webda, Mermilliod (1996).
[3] Extracted from the Canadian Astronomy Data Centre (CADC), at http://cadcwww.dao.nrc.ca/.

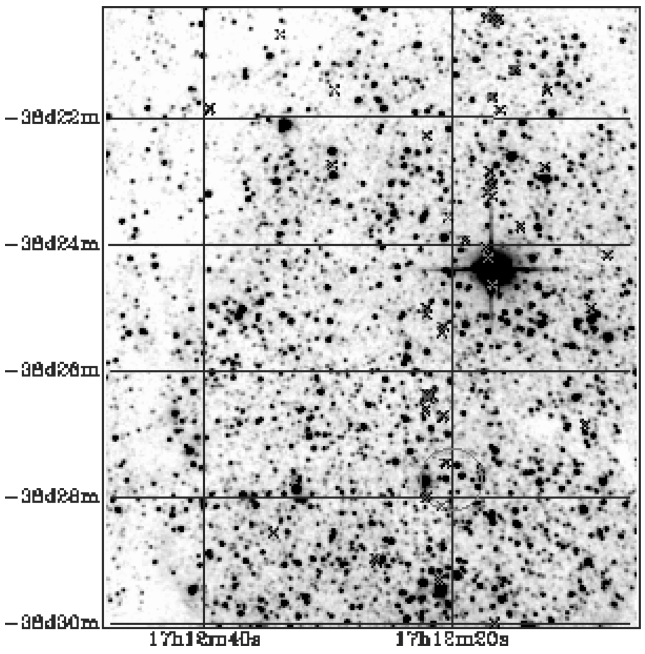

Figure 2. 2MASS 10×10 arcmin^2 K_s image of FSR 1755.

3.1 2MASS photometry

In both cases, J, H and K_s 2MASS photometry was obtained in a relatively wide-circular field of extraction radius $R_{ext} = 50$ arcmin centred on the coordinates provided by FSR (columns 2 and 3 of Table 1) using VizieR.[4] Wide-extraction areas can provide the required statistics, in terms of magnitude and colours, for a consistent field-star decontamination (Section 3.2). They are essential as well to produce stellar RDPs with a high contrast with respect to the background (Section 3.5). In the case of FSR 1603, the RDP resulting from the original FSR coordinates presented a dip at the centre. Thus, we searched for new coordinates to maximize the star counts in the innermost RDP bin. The optimized central coordinates are given in columns 2 and 3 of Table 2. The offset with respect to the original coordinates is relatively small, $\Delta\alpha = -6.0$ arcsec and $\Delta\delta = -32.2$ arcsec.

As a photometric quality constraint, the 2MASS extractions were restricted to stars with errors in J, H and K_s smaller than 0.25 mag. A typical distribution of uncertainties as a function of magnitude, for objects projected towards the central parts of the Galaxy, can be found in Bonatto & Bica (2007b). About 75–85 per cent of the stars have errors smaller than 0.06 mag.

3.2 Colour–magnitude diagrams and field-star decontamination

The CMD morphology is an essential tool to unveil the nature of the stellar overdensities. In the present cases, we use 2MASS $J \times (J - H)$ and $J \times (J - K_s)$ CMDs extracted from a central region that, in the case of star clusters, should provide high-contrast CMDs. However, features present in the central CMDs and in the respective comparison field, show that field stars are an important component in the CMDs (Section 4). Thus, it is essential to quantitatively assess the relative densities of field stars and potential cluster sequences.

To objectively quantify the field-star contamination in the CMDs, we apply the statistical algorithm described in Bonatto & Bica (2007b). It measures the relative number densities of probable field and cluster stars in cubic CMD cells whose axes correspond to the magnitude J and the colours $(J - H)$ and $(J - K_s)$. These are the 2MASS colours that provide the maximum variance among CMD sequences for OCs of different ages (e.g. Bonatto, Bica & Girardi 2004). The algorithm (i) divides the full range of CMD magnitude and colours into a 3D grid, (ii) computes the expected number density of field stars in each cell based on the number of comparison field stars with similar magnitude and colours as those in the cell and (iii) subtracts the expected number of field stars from each cell. By construction, the algorithm is sensitive to local variations of field-star contamination with colour and magnitude. Typical cell dimensions are $\Delta J = 0.5$ and $\Delta(J - H) = \Delta(J - K_s) = 0.25$, which are large enough to allow sufficient star-count statistics in individual cells and small enough to preserve the morphology of different CMD evolutionary sequences. As comparison field, we use the region $R_{lim} < R < R_{ext}$ around the cluster centre to obtain representative background star-count statistics, where R_{lim} is the limiting radius (Section 3.5). Further details on the algorithm, including discussions on subtraction efficiency and limitations, are given in Bonatto & Bica (2007b). The algorithm also gives the parameter $N_{1\sigma}$ which, for a given extraction, corresponds to the ratio of the number of stars in the decontaminated CMD with respect to the 1σ Poisson fluctuation measured in the observed CMD. CMDs of star clusters should have $N_{1\sigma}$ significantly larger than 1.

3.3 Fundamental parameters

Fundamental parameters are derived with solar-metallicity Padova isochrones (Girardi et al. 2002) computed with the 2MASS J, H and K_s filters.[5] The 2MASS transmission filters produced isochrones very similar to the Johnson–Kron–Cousins (e.g. Bessell & Brett 1988) ones, with differences of at most 0.01 in $(J - H)$ (Bonatto et al. 2004).

The isochrone fit gives the age and the reddening $E(J - H)$, which converts to $E(B - V)$ and A_V through the transformations $A_J/A_V = 0.276$, $A_H/A_V = 0.176$, $A_{K_S}/A_V = 0.118$ and $A_J = 2.76 \times E(J - H)$ (Dutra, Santiago & Bica 2002), assuming a constant total-to-selective absorption ratio $R_V = 3.1$. We also compute the distance from the Sun ($d_\odot$) and the Galactocentric distance (R_{GC}), based on the recently derived value of the Sun's distance to the Galactic Centre $R_\odot = 7.2$ kpc (Bica et al. 2006b). Age, A_V, $d_\odot$ and R_{GC} are given in columns 5 to 8 of Table 2, respectively.

3.4 Colour–magnitude filters

Colour–magnitude filters are used to exclude stars with colours compatible with those of the foreground/background field. They are wide enough to accommodate cluster main sequence (MS) and evolved star colour distributions, allowing for the 1σ photometric uncertainties. Colour–magnitude filter widths should also account for formation or dynamical evolution-related effects, such as enhanced fractions of binaries (and other multiple systems) towards the central parts of clusters, since such systems tend to widen the MS (e.g. Hurley & Tout 1998; Kerber et al. 2002; Bonatto, Bica & Santos 2005; Bonatto & Bica 2007b).

[4] vizier.u-strasbg.fr/viz-bin/VizieR?-source=II/246

[5] stev.oapd.inaf.it/∼lgirardi/cgi-bin/cmd

Table 2. Fundamental parameters from this paper.

Target	α (2000) (^{h} ^{m} ^{s})	δ (2000) ($^\circ$ $'$ $''$)	$N_{1\sigma}$	Age (Gyr)	A_V (mag)	$d_\odot$ (kpc)	R_{GC} (kpc)
(1)	(2)	(3)	(4)	(5)	(6)	(7)	(8)
Ru 101, FSR 1603	12:09:45	−62:59:17	6.1 ± 0.8	1.0 ± 0.1	1.7 ± 0.1	2.7 ± 0.2	6.4 ± 0.3
FSR 1755	(‡)	(‡)	5.8 ± 0.9	<5 Myr	≈ 4.1	≈ 1.4	≈ 5.8

Notes. Columns 2 and 3: optimized central coordinates (Section 3.1); (‡) indicates same central coordinates as in FSR. Column 4: ratio of the decontaminated star counts to the 1σ fluctuation level of the observed photometry. Column 6: $A_V = 3.1\,E(B-V)$. Column 8: R_{GC} calculated using $R_\odot = 7.2$ kpc (Bica et al. 2006b) as the distance of the Sun to the Galactic Centre.

However, residual field stars with colours similar to those of the cluster are expected to remain inside the colour–magnitude filter region. They affect the intrinsic stellar radial distribution profile to an extent that depends on the relative densities of field and cluster stars. The contribution of the residual contamination to the observed RDP is statistically taken into account by means of the comparison field.

3.5 Stellar radial density profiles

Star clusters usually have RDPs that follow some well-defined analytical profile. The most often used are the single mass, modified isothermal sphere of King (1966), the modified isothermal sphere of Wilson (1975) and the power law with a core of Elson, Fall & Freeman (1987). Each function is characterized by different parameters that are somehow related to cluster structure. However, considering that errorbars in the present RDPs are significant (see below), and that our goal here is basically to determine the nature of the targets, we decided for the analytical profile $\sigma(R) = \sigma_{bg} + \sigma_0/[1 + (R/R_C)^2]$, where σ_{bg} is the residual background density, σ_0 is the central density of stars and R_C is the core radius. This function is similar to that introduced by King (1962) to describe the surface brightness profiles in the central parts of GCs.

The stellar RDPs are built with colour–magnitude filtered photometry (Section 3.4). Minimization of the presence of non-cluster stars by the colour–magnitude filter results in RDPs with a significantly higher contrast with the background (e.g. Bonatto & Bica 2007b). To avoid oversampling near the centre and undersampling at large radii, RDPs are built by counting stars in rings of increasing width with distance to the centre. The number and width of the rings are adjusted to produce RDPs with adequate spatial resolution and as small as possible 1σ Poisson errors. The residual background level of each RDP corresponds to the average number of colour–magnitude filtered stars measured in the comparison field. The R coordinate (and respective uncertainty) of each ring corresponds to the average position and standard deviation of the stars inside the ring.

We also compute the density contrast parameter $\delta_c = 1 + \sigma_0/\sigma_{bg}$ that measures the intrinsic contrast of a cluster RDP (in the central region) with the background. In general terms, δ_c is a measure of the detectability of clusters by means of star counts. Obviously, the presence of O stars in very young clusters may improve the detectability, even for low δ_c cases. As a caveat, we note that δ_c values measured in colour–magnitude filtered RDPs do not necessarily correspond to the visual contrast produced by optical/IR images. The minimization of field-star contamination produces RDPs with higher contrast than those resulting from the raw photometry (e.g. Bica, Bonatto & Blumberg 2006a).

As a measure of the cluster size, we also derive the limiting radius and uncertainty, which are estimated by comparing the RDP (taking into account fluctuations) with the background level. R_{lim} corresponds to the distance from the cluster centre where RDP and background become statistically indistinguishable. For practical purposes, most of the cluster stars are contained within R_{lim} (Fig. 4). The limiting radius should not be mistaken for the tidal radius; the latter is usually derived from King (or other analytical functions) fits to RDPs, which depend on wide surrounding fields and as small as possible Poisson errors (e.g. Bonatto & Bica 2007b). In contrast, R_{lim} comes from a visual comparison of the RDP and background levels.

The empirical determination of a cluster-limiting radius depends on the relative levels of RDP and background (and respective fluctuations). Thus, dynamical evolution may indirectly affect the measurement of the limiting radius. Since mass segregation preferentially drives low-mass stars to the outer parts of clusters, the cluster/background contrast in these regions tends to lower as clusters age. As an observational consequence, smaller values of limiting radii should be measured, especially for clusters in dense fields. However, simulations of King-like OCs (Bonatto & Bica 2007b) show that, provided not exceedingly high, background levels may produce limiting radii underestimated by about 10–20 per cent. The core radius, on the other hand, is almost insensitive to background levels (Bonatto & Bica 2007b). This occurs because R_C results from fitting the King-like profile to a distribution of RDP points, which minimizes background effects.

4 DISCUSSION

4.1 The IAC nature of FSR 1603

CMDs of the central ($R < 3$ arcmin $\sim 2 \times R_C$) region of FSR 1603 are presented in Fig. 3 (top panels). This extraction contains the bulk of the cluster stars (Fig. 4). Features that stand out are a cluster-like population corresponding to a populous MS [$0.2 \lesssim (J-H) \lesssim 0.6$ and $12.5 \lesssim J \lesssim 16$], a giant clump [$0.6 \lesssim (J-H) \lesssim 0.7$ and $12.2 \lesssim J \lesssim 11$] and a giant branch [$0.7 \lesssim (J-H) \lesssim 1.0$ and $J \lesssim 11$], together with a redder sequence [$(J-H) \gtrsim 0.8$]. Some of these features (especially around the MS and the red component) are present as well in the equal-area comparison field (middle panels), extracted from a ring near 30 arcmin, which suggests some contamination by disc and bulge stars. However, the central and comparison field extractions present significant differences in terms of CMD densities. Besides, the giant clump and giant branch are not present in the comparison field. Similar features are present in the $J \times (J - K_s)$ CMDs (right-hand panels). The qualitative discussion above strongly suggests that FSR 1603 is an intermediate-age OC.

The resulting field-star decontaminated CMDs of FSR 1603 are shown in the bottom panels of Fig. 3. The comparison field was taken from the region $20 \leqslant R \leqslant 50$ arcmin. Bulge and disc contamination have been properly taken into account, except for about

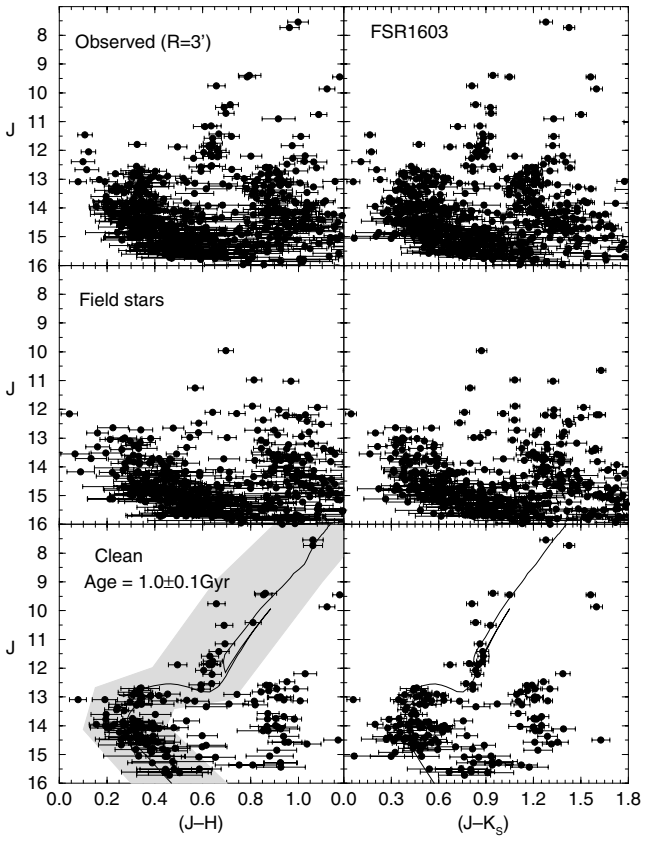

Figure 3. 2MASS CMDs extracted from the $R < 3$ arcmin region of FSR 1603. Top panels: observed photometry with the colours $J \times (J - H)$ (left-hand panel) and $J \times (J - K_s)$ (right-hand panel). Middle panels: equal-area comparison field. Besides some contamination of disc and bulge stars, a populous MS and a conspicuous cluster red giant clump show up in the upper panels. Bottom panels: decontaminated CMDs set with the 1 Gyr Padova isochrone (solid line). The colour–magnitude filter used to isolate cluster MS/evolved stars is shown as a shaded region.

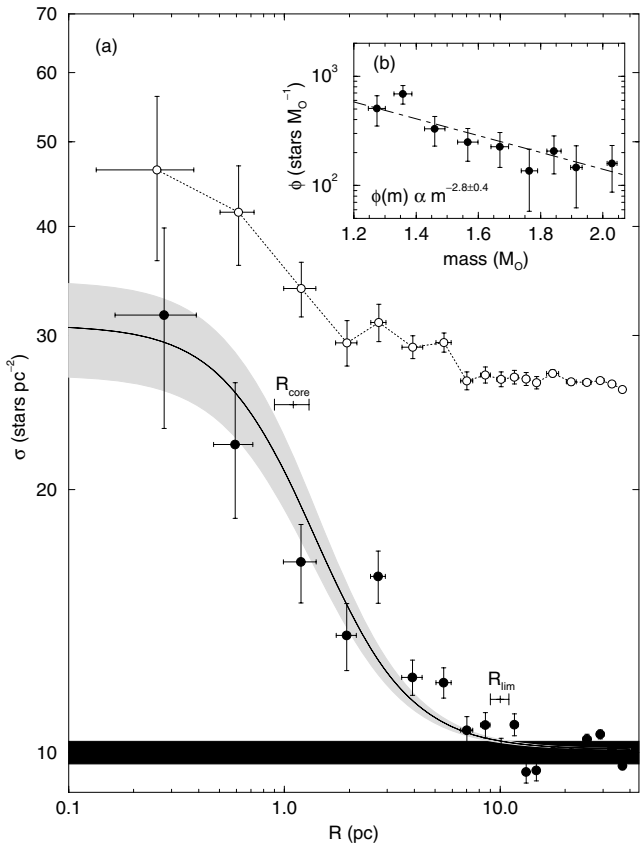

Figure 4. Panel (a): stellar RDP (filled circles) of FSR 1603 built with colour–magnitude photometry. Solid line: best-fitting King profile. Horizontal shaded region: offset field stellar background level. Grey regions: 1σ King fit uncertainty. The core and limiting radii are shown. The RDP built with the observed photometry (open circles) is shown for comparison. Absolute scale is used. Panel (b): field-star decontaminated mass function for the MS stars, fitted with $\phi(m) \propto m^{-2.8}$.

40 red stars that remain in the decontaminated CMDs. Considering that the original red component contains about 214 stars (top panels), the statistical significance of the leftovers represent $N_{1\sigma} = 2.7$, significantly lower than that of stellar sequence identified with FSR 1603 (Table 1). As shown in Bica, Bonatto & Camargo (2007b), such low values of $N_{1\sigma}$ are typical of field fluctuations detected as overdensities by FSR. What emerges from the $N_{1\sigma} = 6.1 \pm 0.8$ decontaminated CMDs are conspicuous sequences, especially the giant clump and the MS, typical of a relatively populous Gyr-class OC.

Indeed, the decontaminated CMD morphology of FSR 1603 is well represented by the 1 Gyr isochrone, with a distance modulus $(m - M)_J = 12.6 \pm 0.1$, and a reddening $E(J - H) = 0.17 \pm 0.01$, which corresponds to $E(B - V) = 0.54 \pm 0.04$ and $A_V = 1.69 \pm 0.12$. Such values imply a distance from the Sun $d_\odot = 2.7 \pm 0.1$ kpc and a Galactocentric distance $R_{GC} = 6.4 \pm 0.2$ kpc. At this distance, the scale is 1 arcmin = 0.774 pc. The isochrone fit to FSR 1603 is shown in the bottom panels of Fig. 3.

Fig. 4 shows the stellar RDP of FSR 1603. Besides the RDP resulting from the colour–magnitude filter, we also show, for illustrative purposes, that produced with the observed (raw) photometry. In both cases, the central region presents a significant density contrast with respect to the background, especially the colour–magnitude filter RDP, with $\delta_c = 3.0 \pm 0.4$. The adopted King-like function describes well the latter RDP throughout the full radii range, within uncertainties. We derive a core radius $R_C = 1.1 \pm 0.2$ pc $= 1.4 \pm 0.3$ arcmin and a limiting radius $R_{lim} = 10 \pm 1$ pc $= 13 \pm 1.3$ arcmin. The central density of stars $\sigma_0 = 20 \pm 4$ stars pc^{-2} and the core radius (R_C) are derived from the RDP fit, while the background level $\sigma_{bg} = 10 \pm 0.3$ stars pc^{-2} is measured in the respective comparison field. The best-fitting solution is superimposed on the colour–magnitude filtered RDP (Fig. 4). Because of the 2MASS photometric limit, which for FSR 1603 corresponds to a cut-off for stars brighter than $J \approx 16$ (Fig. 3), σ_0 should be taken as a lower limit to the actual central number density. Within the uncertainty, the present value of R_C agrees with that given by FSR.

The relatively populous nature of the MS of FSR 1603 can be used to estimate the mass stored in stars. Considering the field-star decontaminated photometry, the number of observed MS and evolved stars for $R < R_{lim}$ amount to $N_{obs}^{MS} = 279 \pm 53$ and $N_{obs}^{Evol} = 46 \pm 10$, respectively. Using the mass–luminosity relation derived from the 1 Gyr Padova isochrone set with the parameters presented above, the observed MS mass is $M_{obs}^{MS} = 407 \pm 46\,M_\odot$. For the evolved stars, we multiply N_{obs}^{Evol} by the stellar mass at the TO ($m_{TO} \approx 2.1\,M_\odot$), which yields the estimate $M_{obs}^{Evol} = 96 \pm 20\,M_\odot$. Thus, the total mass stored in the observed stars of FSR 1603 amounts to $M_{obs} = 503 \pm 50\,M_\odot$.

We also build the mass function (MF) $\phi(m) = \frac{dN}{dm}$, for the MS stars following the methods discussed in Bonatto & Bica (2005). To maximize the statistical significance of field-star counts, we take as the comparison field the region at $15 \leqslant R\,(\mathrm{pc}) \leqslant 39$ that lies $\geqslant 5$ pc beyond the limiting radius. First, we apply the colour–magnitude filter (Fig. 3) to the stars located inside the limiting radius, which eliminates most of the field stars, leaving a residual contamination. We deal with this statistically by building the luminosity functions (LFs) for the cluster and comparison field separately. J, H and K_s LFs are built by counting stars in magnitude bins from the respective faint magnitude limit to the TO. To avoid undersampling near the turn-off and oversampling at the faint limit, magnitude bins are wider in the upper MS than in the lower MS. Correction is made for the different solid angles of the comparison field and cluster region. The intrinsic cluster LF is obtained by subtracting the offset-field LF. Finally, the intrinsic LF is transformed into MF using the mass–luminosity relation obtained from the 1 Gyr Padova isochrone and the observed distance modulus $(m - M)_J = 12.6$. These procedures are applied independently to the three 2MASS bands. The final MF is produced by combining the J, H and K_s MFs. Further details on MF construction are given in Bica et al. (2006a). The resulting MF, covering the mass range $1.27\,\mathrm{M}_\odot \leqslant m_{\mathrm{MS}} \leqslant 2.03\,\mathrm{M}_\odot$, is shown in the inset of Fig. 4, where we also include the fit with the function $\phi(m) \propto m^{-(1+\chi)}$. Within the uncertainty, the slope $\chi = 1.8 \pm 0.4$ is similar to the $\chi = 1.35$ of the Initial Mass Function (IMF) of Salpeter (1955).

Finally, with the above MF we can estimate the total stellar mass in FSR 1603. For masses below the observed lower limit of $1.27\,\mathrm{M}_\odot$, we extrapolate the observed MF down to the H-burning mass limit ($0.08\,\mathrm{M}_\odot$) using the universal IMF of Kroupa (2001). The latter IMF assumes the slopes $\chi = 0.3 \pm 0.5$ for the range $0.08 \leqslant m(\mathrm{M}_\odot) \leqslant 0.5$ and $\chi = 1.3 \pm 0.3$ for $0.5 \leqslant m(\mathrm{M}_\odot) \leqslant 1.0$. With such considerations, the total (extrapolated MS + evolved) mass amounts to $M_{\mathrm{tot}} = (2.3 \pm 0.9) \times 10^3\,\mathrm{M}_\odot$, which implies the average mass density $\rho = 0.55 \pm 0.22\,\mathrm{M}_\odot\,\mathrm{pc}^{-3}$ and the projected density $\sigma = 7.3 \pm 2.9\,\mathrm{M}_\odot\,\mathrm{pc}^{-2}$.

As a caveat, we note that the total mass estimates should be taken as upper limits, since because of dynamical evolution, significant fractions of the low-mass content may have been lost to the field (e.g. Bonatto & Bica 2007a).

4.2 The possible embedded cluster FSR 1755

The images of FSR 1755 (Figs 1 and 2) clearly indicate that this object is a complicated case. Indeed, the differential absorption due to the dust clouds produces conspicuous variations in the stellar number density, as can be seen in Fig. 6.

According to SIMBAD,[6] the bright star at ≈2 arcmin south of the central coordinates of FSR 1755 is the O star CD − 38°11636.

FSR 1755 appears to be spatially associated with the H II region Sh 2-3 (Sharpless 1959), located at α (J2000) = 17:12:21 and δ (J2000) = −38:27:00, also known as Gum 58 (Gum 1955) and RCW 120 (Rodgers, Campbell & Whiteoak 1960). Russeil (2003) provides the radial velocity $v_r = 12.0\,\mathrm{km\,s}^{-1}$ and the kinematic distance $d_\odot = 1.8 \pm 0.7$ kpc for Sh 2-3. According to the spatial distribution of the spiral arms (Russeil 2003), Sh 2-3 appears to be related to the Sagittarius–Carina arm. Sh 2-3 is an optical H II region of dimensions ∼7 arcmin (EW) × 10 arcmin (NS), excited by the O 8V star CD − 38°11636 (LSS 3959), at α (J2000) = 17:12:20.6 and δ (J2000) = −38:29:26. It was identified spectroscopically by Georgelin & Georgelin (1970). Vogt & Moffat (1975) provide $d_\odot = 1.7$ kpc as the photometric distance to this star. CD − 38° 11636 has the apparent magnitudes $B = 11.93$ and $V = 10.79$ (Zavagno et al. 2007), $J = 8.013 \pm 0.021, H = 7.708 \pm 0.036$ and $K_s = 7.523 \pm 0.020$ (2MASS). Based on the optical photometry of CD − 38° 11636, Zavagno et al. (2007) compute $A_V = 4.36$ and estimate the distance to this star as $d_\odot = 1.34$ kpc, which agrees with their kinematic distance of $d_\odot = 1.35$ kpc. With the 2MASS photometry of CD − 38° 11636 and the absolute J and H magnitudes of an O 8V synthetic star (Martins & Plez 2006), we compute $d_\odot = 1.35$ kpc, which agrees with the previous values. We also derive $E(J - H) = 0.4, A_J = 1.14, A_V = 4.15$ and $(m - M)_J = 11.9$.

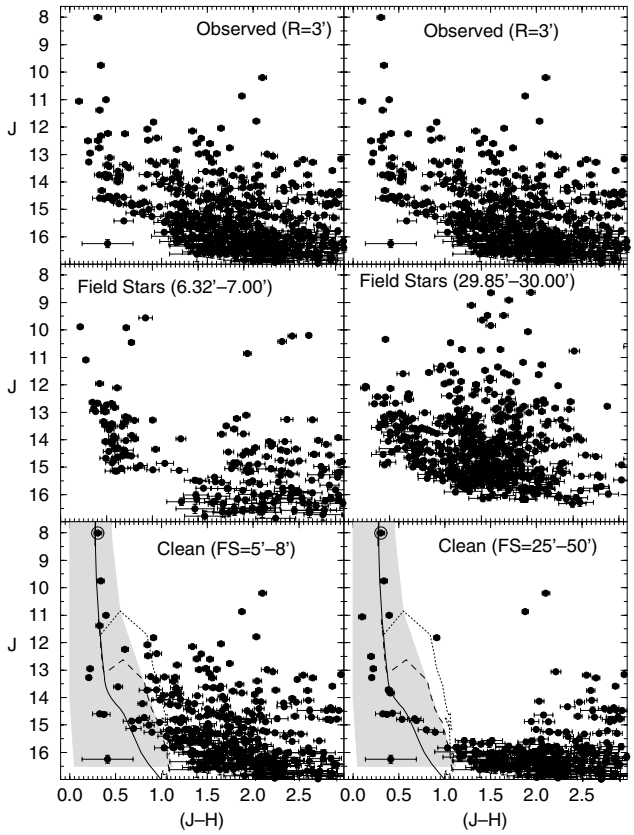

Figure 5. Top panels: $J \times (J - H)$ CMDs of the central $R = 3$ arcmin region of FSR 1755. Middle panels: equal-area comparison fields extracted from two different regions. Bottom panels: CMDs decontaminated using the different comparison fields. The O 8V star CD − 38°11636 is shown by the circle. The 3 Myr Padova isochrone (heavy solid line), together with the 1 Myr (dotted) and 5 Myr (dashed) PMS isochrones have been set for $d_\odot = 1.35$ kpc and $E(B - V) = 1.3$. The shaded region represents the colour–magnitude filter.

In Fig. 5 (top panels), we show the $J \times (J - H)$ CMD extracted from the $R = 3$ arcmin central region of FSR 1755. An almost vertical, blue $[0.05 \lesssim (J - H) \lesssim 0.5, 8 \lesssim J \lesssim 15]$ sequence – typical of very young populations – appears to merge into a dominant concentration of red stars. The strong differential reddening in the field of FSR 1755 hinders the quantitative use of the decontamination algorithm. However, it can be applied as a qualitative probe on CMD features, for different choices of the comparison field. Two cases are examined, one taking field stars from the region $5 \leqslant R \leqslant 8$ arcmin, that basically corresponds to the deep RDP depression (Fig. 6), and the other from an external region $25 \leqslant R \leqslant 50$ arcmin away from

[6] http://simbad.u-starsbg.fr/simbad/

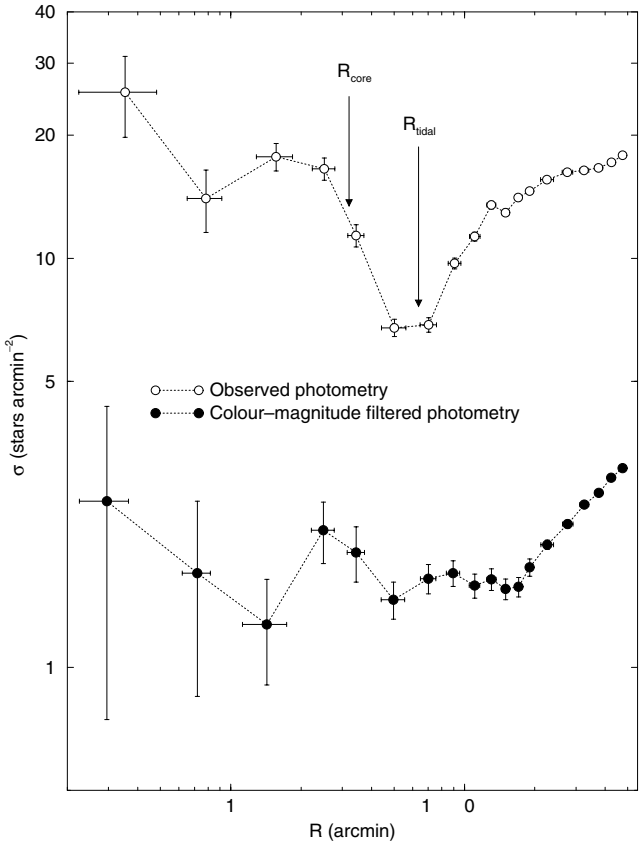

Figure 6. Observed (open circles) and colour–magnitude filtered (filled circles) RDPs of FSR 1755. The core and tidal radii computed by FSR are indicated. The absorption-related depression at $R \approx 5$–7 arcmin helps create the impression of a GC.

the centre. For visual purposes only, we characterize the field contamination on the $R = 3$ arcmin central CMDs, resulting from both choices of comparison field, by means of the equal-area extractions $6.32 \leqslant R \leqslant 7$ arcmin and $29.85 \leqslant R \leqslant 30$ arcmin, respectively. They are shown in the middle panels of Fig. 5. For statistical representativity of the field stars, the decontamination algorithm uses the full radial scale of the adopted comparison fields, $5 \leqslant R \leqslant 8$ arcmin and $25 \leqslant R \leqslant 50$ arcmin, respectively. In both cases, the stellar distributions are similar in terms of colour and magnitudes, but they differ significantly in density.

Consequently, the resulting decontaminated CMDs also present differences, especially in the remaining field-star distribution. However, the blue sequence consistently remains in both CMDs.

Assuming that FSR 1755 is associated with Sh 2-3, we apply to the decontaminated CMDs the 3 Myr Padova isochrone as representative of the young age, together with the preMS (PMS) tracks of Siess, Dufour & Forestini (2000) with the ages 1 and 5 Myr, set for $d_{\odot} = 1.35$ kpc and $E(B-V) = 1.3$. What results in both cases is consistent with a sparse embedded cluster. Thus, most of what remains in the CMDs as the red component results from the strong differential reddening in the rich field. However, because of the strong differential absorption, we cannot exclude the possibility that some fraction of the red component is composed of very reddened PMS stars.

Finally, in Fig. 6 we present the RDPs of FSR 1755. The deep RDP depression, which is due to dust absorption, associated with the large number of stars related to the red component, creates the impression of a high central stellar concentration and large core radius. Taken together, these features match the GC criterion established by FSR. Indeed, the RDP dip (Fig. 6) coincides with the tidal radius computed by FSR.

On the other hand, most of the above features are absent in the colour–magnitude filtered RDP, which has a low-level central concentration of stars typical of a poorly populated star cluster and a small bump at $R \approx 2.5$ arcmin that coincides with the radial distance of CD $-38^{\circ}11636$.

From the above, we conclude that the potentially populous cluster FSR 1755 is in fact an artefact produced by the highly spatially variable star-count density and absorption across the field. However, we cannot exclude the possibility of a sparse young cluster embedded in the H II region Sh 2-3.

5 SUMMARY AND CONCLUSIONS

In this paper, we investigated the nature of the GC candidates FSR 1603 and FSR 1755, taken from the FSR catalogue, by means of decontaminated J, H and K_s 2MASS CMDs and stellar RDPs. Both objects were originally classified as GC candidates by FSR based essentially on the number of cluster stars, the core radius and the central star density. Basically, what results from this work is that neither object is in fact a GC: FSR 1603 is a populous intermediate-age OC and FSR 1755 may consist of a sparse young cluster embedded in a complex H II region.

FSR 1603 corresponds to the OC Ruprecht 101, for which cluster parameters were derived for the first time. It is a massive IAC, with age $= 1.0 \pm 0.1$ Gyr, located at $d_{\odot} = 2.7 \pm 0.2$ kpc from the Sun and Galactocentric distance $R_{GC} = 6.3 \pm 0.3$ kpc, reddening $E(B-V) = 0.54 \pm 0.04$, core and limiting radii $R_C = 1.1 \pm 0.2$ pc and $R_{lim} = 10 \pm 1$ pc, respectively. The mass stored in the observed stars is $M_{obs} \approx 500\,M_{\odot}$; extrapolation to the low-MS stars ($\sim 0.08\,M_{\odot}$) increases the mass to $M_{tot} \sim 2300\,M_{\odot}$. Ru 101 was probably misclassified as a GC candidate because it is a populous OC.

FSR 1755 is related to the optical H II region Sh 2-3, located at $d_{\odot} \approx 1.4$ kpc. The object is surrounded both by H α emission and dust absorption even in the K_s band. A nearly vertical, blue CMD sequence, that includes the O 8V star CD $-38^{\circ}11636$, appears to define FSR 1755 as a sparse embedded cluster. Because of the strong differential reddening in the surroundings, a large number of red stars show up in the CMDs, which probably produced the stellar enhancement that was taken as GC candidate by FSR. We conclude that the GC identification of FSR 1755 is a dust-absorption artefact in a very rich stellar field.

Systematic surveys such as that of FSR are important to detect new star cluster candidates throughout the Galaxy. Nevertheless, works like the present one, that fine tune the analysis by means of field-star decontaminated CMDs and stellar radial profiles, turn out to be fundamental to probe the nature of such candidates, especially those projected against dense stellar fields.

ACKNOWLEDGMENTS

We thank the anonymous referee for suggestions. We acknowledge partial support from CNPq (Brazil). This research has made use of the SIMBAD data base, operated at CDS, Strasbourg, France, as well as of data products from the Two-Micron All-Sky Survey (2MASS), which is a joint project of the University of Massachusetts and the Infrared Processing and Analysis Centre/California Institute of Technology, funded by the National Aeronautics and Space Administration and the National Science Foundation. We employed Digitized

Sky Survey images from the Space Telescope Science Institute (US Government grant NAG W-2166) obtained using the extraction tool from CADC (Canada). We also made use of the WEBDA data base, operated at the Institute for Astronomy of the University of Vienna.

REFERENCES

Bessell M. S., Brett J. M., 1988, PASP, 100, 1134
Bica E., Bonatto C., Blumberg R., 2006a, A&A, 460, 83
Bica E., Bonatto C., Barbuy B., Ortolani S., 2006b, A&A, 450, 105
Bica E., Bonatto C., Ortolani S., Barbuy B., 2007a, A&A, 472, 483
Bica E., Bonatto C., Camargo D., 2007b, MNRAS, in press (astro-ph/0712.0762)
Binney J., Merrifield M., 1998, Galactic Astronomy. Princeton Univ. Press, Princeton, NJ
Bonatto C., Bica E., 2005, A&A, 437, 483
Bonatto C., Bica E., 2007a, A&A, 473, 445
Bonatto C., Bica E., 2007b, MNRAS, 377, 1301
Bonatto C., Bica E., 2007c, A&A, in press (astro-ph:0711.1434)
Bonatto C., Bica E., Girardi L., 2004, A&A, 415, 571
Bonatto C., Bica E., Santos J. F. C., Jr, 2005, A&A, 433, 917
Bonatto C., Bica E., Ortolani S., Barbuy B., 2007, MNRAS, 381, L45
Dutra C. M., Santiago B. X., Bica E., 2002, A&A, 383, 219
Elson R. A. W., Fall S. M., Freeman K. C., 1987, ApJ, 323, 54
Froebrich D., Meusinger H., Scholz A., 2007a, MNRAS, 377, L54
Froebrich D., Scholz A., Raftery C. L., 2007b, MNRAS, 374, 399 (FSR)
Froebrich D., Meusinger H., Davis C. J., 2008, MNRAS, 383, L45
Georgelin Y. P., Georgelin Y. M., 1970, A&AS, 3, 1
Girardi L., Bertelli G., Bressan A., Chiosi C., Groenewegen M. A. T., Marigo P., Salasnich B., Weiss A., 2002, A&A, 391, 195
Gum C. S., 1955, Mem. R. Astron. Soc., 67, 155
Hurley J., Tout A. A., 1998, MNRAS, 300, 977
Kerber L. O., Santiago B. X., Castro R., Valls-Gabaud D., 2002, A&A, 390, 121
King I., 1962, AJ, 67, 471
King I., 1966, AJ, 71, 64
Kroupa P., 2001, MNRAS, 322, 231
Martins F., Plez B., 2006, A&A, 457, 637
Mermilliod J. C., 1996, in Milone E. F., Mermilliod J.-C. eds, ASP Conf. Ser. Vol. 90, The Origins, Evolution and Destinies of Binary Stars in Clusters. Astron. Soc. Pac., San Francisco, p. 475
Rodgers A. W., Campbell C. T., Whiteoak J. B., 1960, MNRAS, 121, 103
Russeil D., 2003, A&A, 397, 133
Salpeter E., 1955, ApJ, 121, 161
Sharpless S., 1959, ApJS, 4, 257
Siess L., Dufour E., Forestini M., 2000, A&A, 358, 593
Vogt N., Moffat A. F. J., 1975, A&A, 45, 405
Wilson C. P., 1975, AJ, 80, 175
Zavagno A., Pomarès M., Deharveng L., Hosokawa Y., Russeil D., Caplan J., 2007, A&A, 472, 835

This paper has been typeset from a TEX/LATEX file prepared by the author.